atom.[40] Repulsive exchange interactions between methyl and the filled orbitals of the ligands accounts for the ligand effect. But ths is only the quantum mechanical way of describing steric strain.[41]

It is interesting that increasing the positive charge on the metal atom will greatly strengthen the methyl–metal bond relative to hydrogen.[40,42] This is just the result expected since the metal becomes a harder Lewis acid, and now prefers the harder CH_3^- ligand over H^-. In more elegant language, positive charge on the metal contracts its d orbitals, and reduces the repulsive exchange effects.

Conclusions

It appears to be possible to obtain relative values of local hardness for Lewis acids and bases, which are both rational and consistent. Furthermore, such values, obtained from bond energy differences, are in reasonable agreement with relative values of $\eta = (I - A)/2$. They also show that the chemical hardness of anions, not directly measureable, is not greatly different from that of related neutral molecules.

The consistency suggests that eq 4 is usually reliable and my have useful applications. Exceptions do occur but seem to have reasonable explanations such as steric strain or cross-conjugation. Hydride ion is a special case among bases. It is actually surprising that specific properties are not invoked more often.

The relative hardness values of F^-, OH^-, NH_2^-, and CH_3^- seem to be well correlated with the extent to which their valence shell electrons can produce π-repulsions with the filled valence shells of Lewis acids. Going down a series such as F^-, Cl^-, Br^-, I^-, these repulsions are diminished and eventually beome net stabilizations.[43-44]

Finally, it should be mentioned that there is a rapidly growing literature on the modern meaning of chemical hardness. Some of these articles give tables of η, or η, which may be compared with those presented here.[51]

Acknowledgment. This work was supported by the U.S. Department of Energy (Contract No. DEAS03-76SF0034).

(40) Ziegler, T.; Tschinke, V.; Becke, A. *J. Am. Chem. Soc.* **1987**, *109*, 1351-1358.
(41) Halpern, ref 39, has experimental evidence for steric strain.
(42) Armentrout, P. G.; Halle, L. F.; Beauchamp, J. L. *J. Am. Chem. Soc.* **1981**, *103*, 6501-6502.
(43) Mulliken, R. S. *J. Am. Chem. Soc.* **1955**, *77*, 884-887.
(44) Simple polarization also accounts for a stabilization of soft–soft pairs: Bernardi, F.; Bottone, A.; Venturini, A.; Mangini, A. *J. Am. Chem. Soc.* **1986**, *108*, 8171-8175.
(45) Rosenstock, H. M.; Draxl, K.; Steiner, B. W.; Herron, J. T. *J. Phys. Chem. Ref. Data* **1977**, *6*, Suppl. 1.
(46) Moore, C. E. *Ionization Potentials and Ionization Limits*; Natl. Stand. Ref. Data Ser. No 34; National Bureau of Standards: Washington, D.C., Sept 1970.
(47) Drzaic, P. S.; Marks, J.; Brauman, J. I. *Gas Phase Ion Chemistry*; Bowers, M. T., Ed.; Academic Press: New York, 1984; Vol. 3, Chapter 21.
(48) DePuy, C. H.; Bierbaum, V. M.; Damrauer, R. *J. Am. Chem. Soc.* **1984**, *106*, 4051-4053.
(49) Stull, D. R.; Westrum, Jr., E. F.; Sinke, G. C. *The Chemical Thermodynamics of Organic Compounds*; Wiley: New York, 1969.
(50) Pearson, R. G. *J. Org. Chem.* **1987**, *52*, 2131-2136.
(51) See: Bergmann, D.; Hinze, J. In *Electronegativity*; Sen, K. D., Jorgensen, C. K., Eds.; Springer-Verlag: Berlin, 1987. Komorowski, L. *Chem. Phys.*, Lett. **1987**, *134*, 536-540.

Dynamics of Ligand Escape from the Heme Pocket of Myoglobin

J. Kottalam and David A. Case*

Contribution from the Department of Molecular Biology, Research Institute of Scripps Clinic, 10666 North Torrey Pines Road, La Jolla, California 92037. *Received April 18, 1988*

Abstract: Molecular dynamics calculations are used to study the kinetics of the process by which a dioxygen ligand leaves the heme pocket of sperm whale myoglobin. Umbrella sampling techniques are used to generate free-energy profiles at several temperatures for escape along a path between the distal histidine and valine residues, and methods for assessing the statistical precision of such profiles are explored. The results are used to compute rate constants for ligand escape, both in the transition-state approximation and with full classical dynamics. Corrections to transition-state theory rates (i.e., the transmission coefficients) are in the range 0.8 to 0.9 for this process, and the computed rate constants at room temperature are in good agreement with experiment. Near room temperature the computed activation energy is less than 1 kcal/mol, but at lower temperatures (between 180 and 270 K) this rises to 5 kcal/mol. Potential physical origins of such non-Arrhenius temperature dependence are discussed in light of models of protein fluctuations that accompany ligand escape.

The study of the binding of gaseous ligands to heme proteins has served for many years as an important test case of our ability to understand enzyme–substrate interactions in general. Aside from the simplicity of the ligands (such as O_2, CO, or NO), and the wealth of structural data available for heme proteins, these systems have the important advantage that they can be followed over a wide time domain following photodissociation of the ligand by a short laser pulse. Intermediates in the ligand rebinding process were originally identified in low-temperature studies,[1] and have recently been characterized at room temperature as well.[2]

There is general agreement that the main features of ligand binding to myoglobin can be described by a (phenomenological) kinetic scheme with two or three intermediate states:[1,2]

$$MbL \rightleftharpoons \text{"B"} \rightleftharpoons \text{"C"} \rightleftharpoons Mb + L$$

Here, state B has the ligand molecule inside the protein matrix, presumably near the heme group, but not bound to the iron atom.

(1) Austin, R. H.; Beeson, K. W.; Eisenstein, L.; Frauenfelder, H.; Gunsalus, I. C. *Biochemistry* **1975**, *14*, 5355.
(2) (a) Henry, E. R.; Sommer, J. H.; Hofrichter, J.; Eaton, W. A. *J. Mol. Biol.* **1983**, *166*, 443. (b) Gibson, Q. H.; Olson, J. S.; McKinnie, R. E.; Rohlfs, R. J. *J. Biol. Chem.* **1986**, *261*, 10228. (c) Olson, J. S.; Rohlfs, R. J.; Gibson, Q. H. *J. Biol. Chem.* **1987**, *262*, 12930. (d) Jongeward, K. A.; Magde, D.; Taube, D. J.; Marsters, J. C.; Traylor, T. G.; Sharma, V. S. *J. Am. Chem. Soc.* **1988**, *110*, 380.

0002-7863/88/1510-7690$01.50/0

State C is distinct from B, but still has the ligand embedded in the protein, either outside the heme pocket or in a (kinetically) distinct position within the heme pocket. (This scheme omits additional intermediates thay may be required to explain observations at short times or low temperatures, but which are not kinetically resolvable near room temperature.[1]) For myoglobin (but not for hemoglobin) the spectral characteristics of states B and C are virtually identical with those of deoxymyoglobin; i.e., the heme group relaxes in less than 10 ns to a deoxy-like conformation.[3] This simplifies the kinetic analysis since ligand migration in the protein matrix (which is the process of interest here) takes place on much longer time scales.

Even for situations where the phenomenological kinetic analysis is straightforward, a significant challenge remains to interpret the observed intermediates in terms of the stereochemistry of the myoglobin molecule. Each of the intermediates in the simple linear scheme given above probably represents multiple ligand or protein conformations that differ slightly in their exact geometries, and which may interconvert rapidly at room temperature; this interpretation is supported by X-ray crystallographic and low-temperature kinetic studies that show multiple conformations of both bound and photodissociated CO.[4] A variety of theoretical simulations have been undertaken to study the response of the ligand and protein to photodissociation,[5] and to locate possible pathways into and out of the heme pocket.[6] It is important that models such as these be tested against experimental kinetic data. Here we present results of rate constant calculations (over a wide temperature range) for one plausible model for the way in which a diatomic ligand escapes from the heme pocket in myoglobin. The results are of interest in their own right, and point the way to similar calculations on alternative models that should help to delineate the range of microscopic models that are consistent with the observed kinetics.

The basic simulation procedure consists of computing both the transition-state theory estimate of the ligand escape rate, and dynamical corrections to it, at several temperatures from 180 to 330 K. In the next section, we outline the procedures we use and describe our model for state "C" and the pathway connecting it to the solvent. Results are presented in the following section, with estimates of our statistical uncertainties and comparisons with experimental data. The final section discusses the implications of our model for understanding the ligand binding process and considers potential future calculations.

Method of Computation

1. A Trial Pathway for Ligand Escape. It has been recognized for about 20 years that the ligand binding "pocket" in hemoglobin and myoglobin is inaccessible to small ligands if the protein is maintained in its X-ray conformation,[7] leading to the notion that ligand binding must be accompanied by the transient opening of a "gate" of protein atoms to permit access. Dynamical simulations of the migration of small molecules within the myoglobin matrix have suggested that a variety of paths may permit such access;[6] the simplest such path, and the one that has received the greatest theoretical attention, lies approximately parallel to the heme plane, passing between the side chains of Val E11 and His E7. This path is illustrated in Figure 1, which shows the energetics of a test sphere in the presence of myoglobin in its X-ray conformation.

Although there is no direct evidence showing ligand escape along this general path, several features recommend it for initial detailed simulations: it is the shortest and most direct path for ligand escape, and can be "opened" by energetically feasible movements of the side chains of E7, E10, and E11;[6] when myoglobin is prepared with a phenyl group attached to the iron, this bulky ligand lies along a crevice near His E7;[8] in CO myoglobin, the side chain of Arg CD3 is found to be disordered, such that in the "alternate" conformation it moves away from His E7, which should allow greater freedom of motion for that side chain.[9]

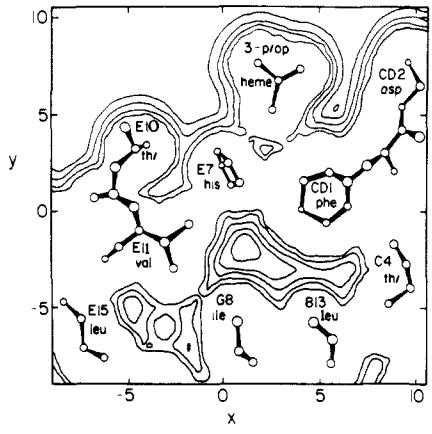

Figure 1. Contour map of energy seen by a ligand in a plane through the X-ray structure of myoglobin. In this coordinate system, the heme group is in the *xy* plane, with the iron atom at the origin. Contours are at 90, 30, 10, 0, and −5 kcal/mol relative to a ligand at infinity; contours closest to the atom positions are at 90 kcal/mol.

Table I. List of Residues Included in the Active Site

Leu	B10	Leu	B13	Phe	B14	Thr	C4
Lys	C7	Phe	CD1	Arg	CD3	Phe	CD4
His	E7	Gly	E8	Val	E9	Thr	E10
Val	E11	Leu	E12	Ala	E14	Leu	F4
Ser	F7	His	F8	His	FG2	Ile	FG4
Leu	G5	Ile	G8	Phe	H15	Heme$^+$	O_2

In order to follow the motion along this path, we define a reaction coordinate, δ, that changes as one passes through the "bottleneck" region between E7 and E11. As we discuss below, the final rate constant estimates will be independent of this choice if the sampling of phase space is adequate. We define δ as the perpendicular distance from the center of mass of the dioxygen ligand to the plane defined by C_β of Val E11, $C\gamma$ of His E7, and the nitrogen of pyrrole 1 of the heme group. The orientation is such that negative values are inside the protein, and positive values toward the outside. As we show below, the bottleneck (i.e., the maximum in the free energy profile) occurs at about $\delta^+ = -0.5$ Å, slightly to the inside of the plane containing the three atoms listed above. Further mathematical details have been given earlier.[10]

2. Active-Site Simulations. As discussed below, molecular dynamics simulations are used to estimate the rate of oxygen escape along this pathway. In order to reduce the computational requirements, we have chosen to simulate directly only an "active site" of residues within a 12-Å radius of the initial oxygen position; these amino acids are listed in Table I. The remainder of the protein undergoes Langevin dynamics that reproduces its average thermal motion and allows energy to flow into and out of the active-site region. Our implementation is nearly the same as that described by Brooks et al.[11]

Specifically, in the reaction region, all atoms feel the usual forces from other atoms, both in the reaction region and from a buffer zone, which in our case comprises the remainder of the protein.

(3) Findsen, E. W.; Scott, T. W.; Chance, M. R.; Freidman, J. M.; Ondrias, M. R. *J. Am. Chem. Soc.* **1985**, *107*, 3355. Sassaroli, M.; Rousseau, D. L. *Biochemistry* **1987**, *26*, 3092.

(4) Fiamingo, F. G.; Alben, J. O. *Biochemistry* **1985**, *24*, 7964. Kuriyan, J.; Wilz, S.; Karplus, M.; Petsko, G. *J. Mol. Biol.* **1986**, *192*, 133. Ansari, A.; DiIorio, E. E.; Dlott, D. D.; Frauenfelder, H.; Iben, I. E. T.; Langer, P.; Roder, H.; Sauke, T. B.; Shyamsunder, E. *Biochemistry* **1986**, *25*, 3139.

(5) Sassaroli, M.; Rousseau, D. L. *J. Biol. Chem.* **1986**, *261*, 16292.

(6) Case, D. A.; Karplus, M. *J. Mol. Biol.* **1979**, *132*, 343. Tilton, R. F., Jr.; Singh, U. C.; Weiner, S. J.; Connolly, M. L.; Kuntz, I. D., Jr.; Kollman, P. A.; Max, N.; Case, D. A. *J. Mol. Biol.* **1986**, *192*, 443.

(7) Perutz, M. F.; Matthews, F. S. *J. Mol. Biol.* **1966**, *21*, 199.

(8) Ringe, D.; Petsko, G. A.; Kerr, D.; Ortiz de Montellano, P. R. *Biochemistry* **1984**, *23*, 2.

(9) Kuriyan, J. A.; Wilz, S.; Karplus, M.; Petsko, G. A. *J. Mol. Biol.* **1986**, *192*, 133. Kuriyan, J.; Karplus, M.; Petsko, G. A. *Proteins: Str., Func. Gen.* **1987**, *2*, 1.

(10) Case, D. A.; McCammon, J. A. *Proc. N.Y. Acad. Sci.* **1986**, *482*, 222.

(11) Brooks, C. L., III; Brunger, A.; Karplus, M. *Biopolymers* **1985**, *24*, 843.

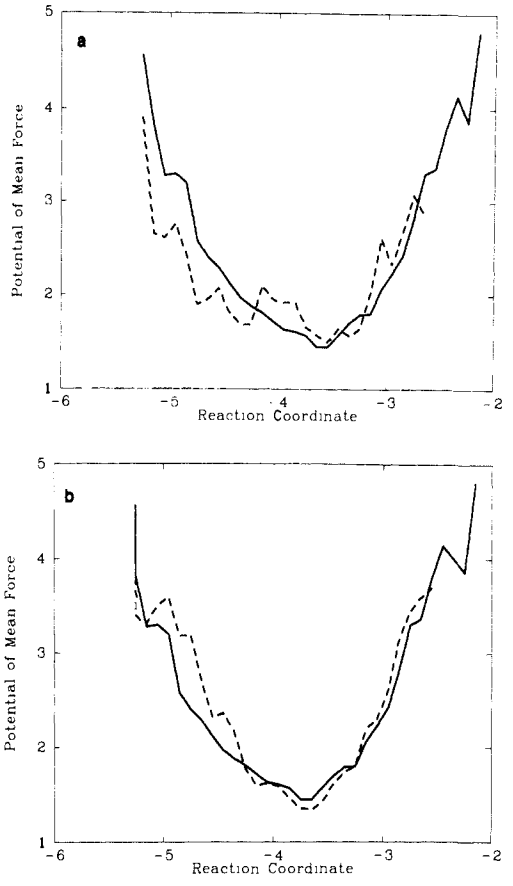

Figure 2. Comparison of potentials of mean force from trajectories of different lengths: solid line, 90-ps simulation; dashed lines, (a) 10-ps, (b) 40-ps simulation.

Atoms in the buffer zone are constrained to their mean positions through harmonic restoring forces and are acted upon by random Langevin forces and the corresponding friction terms; their equation of motion is thus:

$$m\ddot{\mathbf{x}} = -\mathbf{F}(\mathbf{x}) - \Omega(\mathbf{x} - \mathbf{x}_0) - m\gamma\dot{\mathbf{x}} + \mathbf{f}(t) \quad (1)$$

Here Ω is the strength of the restoring force that keeps the buffer atoms near the equilibrium positions $\mathbf{x}_0$, $\mathbf{F}(\mathbf{x})$ are the forces arising from interactions with the active site atoms, γ is a friction coefficient, and $\mathbf{f}(t)$ is a white noise term, i.e., a Gaussian random variable with zero mean and correlation function

$$\langle \mathbf{f}(t)\mathbf{f}(t') \rangle = 2mk_B T\gamma\delta(t - t') \quad (2)$$

The fluctation–dissipation relation 2 ensures that the buffer will undergo fluctuations appropriate to temperature T. The active site atoms will be in rough equilibrium with the buffer, eliminating the need to control their temperature through artificial constant-temperature algorithms that are often employed. Methods for numerically integrating eq 1 have been discussed by Berendsen,[12] and further details of our implementation (into the AMBER 3.0[13] group of programs) will be presented elsewhere. Following Brooks et al.,[11] we have used Ω = 10 kcal/mol-Å^2 and γ = 50 ps^{-1} for all the calculations reported here.

The "success" of such a partitioning procedure fundamentally lies in having the active site zone large enough that details of the motion in the buffer region are unimportant. In a previous calculation, we kept the buffer region frozen, which should be a more severe approximation than that employed here. Nevertheless, our computed free energy barrier for ligand escape (see below) at 300 K was the same within 0.5 kcal/mol for the two simulations,

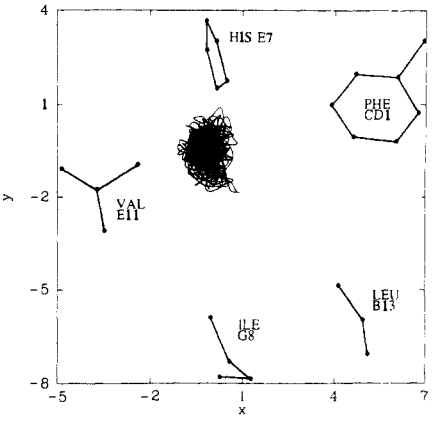

Figure 3. Trajectory of the dioxygen center of mass from a 100-ps simulation. This is a projection on the xy plane of the coordinate system of Figure 1, i.e., a projection on the heme plane.

Table II. Parameters for Umbrella Potentials.

window no.	δ (Å)	K (kcal/mol)	window no.	δ (Å)	K (kcal/mol)
1	−2.5	2.5	6	0.5	5.0
2	−2.0	4.0	7	1.0	5.0
3	−1.5	5.0	8	1.5	4.0
4	−1.0	5.0	9	2.0	4.0
5	−0.5	2.5	10	2.5	2.5

supporting the notion that our current active site model is large enough to show realistic dynamics. Future calculations will explore the implications of larger and smaller active site regions, and of adding solvent to the simulation.

All of the calculations used the AMBER united atom potential energy functions,[14] with porphyrin parameters defined by fits to observed vibrations in metalloporphyrins,[15] and ligand parameters described earlier.[10] In this potential energy function, the dioxygen ligand is dissociated from the iron atom and is not allowed to rebind; the porphyrin parameters are those appropriate to a deoxy state, since spectroscopic evidence indicates that this state is obtained within a few nanoseconds of photolysis at room temperature;[3] the ligand escape trajectories of interest here occur on much longer time scales.

3. Potentials of Mean Force. Our initial simulation began with the dissociated ligand in the heme pocket. An initial energy-minimized structure was slowly heated to 300 K over 20 ps, then equilibrated at that temperature for an additional 20 ps. This was followed by 100 ps of dynamics, during which time the ligand remained in the heme pocket, and the reaction coordinate δ remained in the range $-5.5 < \delta < -2.5$. The distribution of δ values over this trajectory, $\rho(\delta)$, was determined using bins 0.1 Å wide, and from the potential of mean force $W(\delta) = -k_B T \ln \rho(\delta)$, as shown in Figure 2. Figure 3 shows the actual trajectory of the center of mass of the dioxygen ligand, projected onto a plane parallel to the heme group; the average positions of some of the adjoining residues that define the "heme pocket" are also indicated.

Figure 2 also compares the potential of mean force for the full run with distributions sampled from portions of it. It is clear that the resulting potential has converged excellently after 40 ps, and even the 10-ps simulations are fairly reliable, although there are some differences greater than 0.5 kcal/mol, compared to the full 100-ps results. Accuracy of these functions, especially near their end points, is important if they are to be adequately matched to other potentials, as discussed next.

Since the barrier to escape toward more positive values of δ is not known a priori, we carried out an initial series of calculations with strong biassing potentials $U(\delta) = K(\delta - \delta_0)^2$, where K and δ_0 vary as indicated in Table II. Each "window" began from the

(12) VanGunsteren, W. F.; Berendsen, H. J. C.; Rullmann, J. A. C. *Mol. Phys.* **1982**, *45*, 637.
(13) Singh, U. C.; Caldwell, J.; Kollman, P. A. AMBER 3.0 Programs, University of California, San Francisco.
(14) Weiner, S. J.; Kollman, P. A.; Case, D. A.; Singh, U. C.; Ghio, C.; Alagona, G.; Profeta, A., Jr.; Weiner, P. *J. Am. Chem. Soc.* **1984**, *106*, 765.
(15) Giammona, D. A. Ph.D. Thesis, University of California, Davis, 1985.

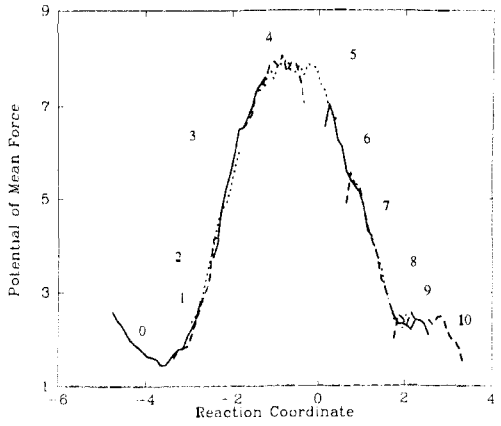

Figure 4. Matched pieces of the potential of mean force from a series of constrained dynamics with umbrella potentials of Table II.

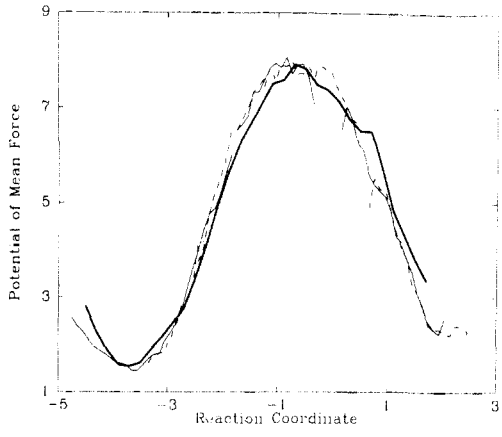

Figure 5. The potential of mean force from a long (100 ps) single trajectory with an umbrella potential given in eq 4 (heavy line). It is compared with that obtained by the conventional piecewise manner (light lines).

end point of the previous simulation, and consisted of 5 ps of equilibration in the new $U(\delta)$, followed by 10 ps of sampling. The equilibrium distribution $\rho^*(\delta)$ in the presence of the biassing potential can be related to the potential of mean force by:

$$W(\delta) = -k_B T \ln [\rho^*(\delta)] - U(\delta) + C_i \qquad (3)$$

where C_i is a different constant for each window. Since the distributions for the various windows overlap, the potentials of mean force can be joined to form a continuous function, and this procedure determines the constants C_i. The resulting profile is shown in Figure 4, indicating a free energy barrier of about 7 kcal/mol at 300 K toward escape to the solvent. This is close to the value we obtained in our preliminary study,[9] which used shorter equilibration times and a different model for the connection between the bath and the reservoir atoms.

Once an initial estimate of the free energy profile is available, a new biassing potential can be chosen that approximately cancels the barrier over the entire region of δ, and allows a large portion of the configuration space to be sampled in a single simulation. We chose the form:

$$U(\delta) = -6.5 + 1.1(\delta + 0.65)^2 \quad \text{if } \delta > -3.08$$
$$U(\delta) = 0 \quad \text{otherwise} \qquad (4)$$

After an initial equilibration, 100 ps of dynamics with this $U(\delta)$ was used to determine $W(\delta)$, as shown in Figure 5. The agreement with the profile determined initially with several overlapping "windows" is excellent, showing that we obtain the same profile with different biassing potentials, which should be the case if the sampling of configuration space is adequate. Figure 6 shows the time course of $\delta(t)$ over this run. More than 30 "transitions" across the bottleneck region around $\delta = -0.5$ are observed, supporting the notion that a statistically valid ratio of residence times on both

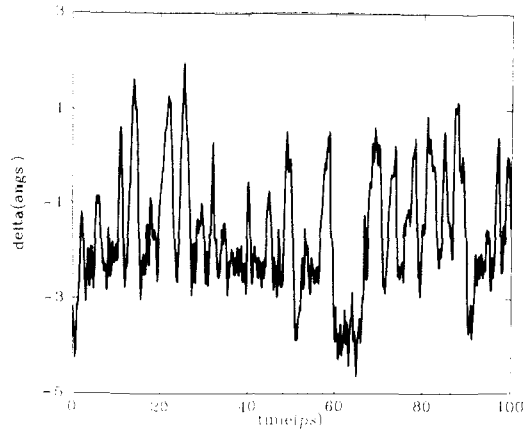

Figure 6. Trajectory of the reaction coordinate during the long (100 ps) dynamics using eq 4.

sides of the bottleneck can be determined from this simulation. With these (relatively long) sampling times, the height of the free energy barrier can be determined with a statistical error of less than 0.5 kcal/mol. This is important if temperature effects are to be reliably estimated, as we discuss next.

4. Effects of Temperature. One of the most interesting features of the rebinding of photodissociated ligands to myoglobin is its behavior at low temperatures. For dioxygen, below about 240 K, the rate for escape into solvent is so slow that the ligand is effectively trapped inside the protein matrix. Between 240 and 320 K, escape does occur, at a rate which Austin et al.[1] fit to an Arrhenius plot with E_a = 12.5 kcal/mol and $A = 10^{15.0}$ s^{-1}. At 20 °C, the rate of this escape (process C → E in the notation of ref 1; see also Figure 19 of that paper) extrapolates to 5×10^5 s^{-1}, in a 3:1 v/v glycerol–water mixture. This is significantly different from the value of $(1.4 + 1.0) \times 10^7$ s^{-1} estimated by Gibson et al.[2b] in 0.1 M phosphate at 20 °C, or the value of 1.3×10^7 s^{-1} deduced[2] from transient work by Duddel et al.,[16] or the value of $0.88 + 0.16 \times 10^7$ s^{-1} observed in recent picosecond studies.[2d] (Some portion of this difference is probably due to the differences in solvent conditions; Olson et al.[2c] report that escape of CO from the heme pocket of hemoglobin β chains is about three times slower in 75% glycerol than in water. Other sources of uncertainty include assumptions about the intrinsic quantum yield of the photodissociation process and inevitable difficulties in temperature extrapolations.) Furthermore, our earlier simulations had suggested that a significant portion of the barrier to escape arises from a negative entropy of activation, which might imply a smaller temperature dependence of the rate constant than that seen by the Frauenfelder group. In order to gain more insight into this gating behavior at low temperatures, we decided to repeat the simulation procedure described above at a series of temperatures.

We have carried out simulations analogous to those described above at 180, 210, 240, 270, 300, and 330 K. The resulting potentials of mean force are shown in Figure 7. The general shapes of the curves are preserved, but it is clear that the barrier height increases with temperature throughout this range. This would be expected if the activation entropy were negative, as we predicted from our earlier calculations.[10] A detailed interpretation of this temperature behavior requires estimates of rate constants at the various temperatures, which is the subject of the next two sections.

5. Transition-State Theory Rates. Once the equilibrium distributions are known, the transition-state theory estimate of the rate constant can be readily calculated:

$$k_{TST} = (1/2)(|d\delta/dt|)_{eq}\left\{\rho(\delta^+)\left[\int \rho(\delta)\, d\delta\right]^{-1}\right\} \qquad (5)$$

Here the time derivative of δ is evaluated from an equilibrium

(16) Duddell, D. A.; Morris, R. J.; Muttucumaru, N. J.; Richards, J. T. *Photochem. Photobiol.* **1980**, *31*, 479.

Table III. Calculation of Kinetic Parameters at Several Temperatures

temp, K	$^1/_2\langle\lvert d\delta/dt\rvert\rangle_{eq}$ (cm/s)	$-W(\delta^*)$ (kcal/mol)	$\int_{-4.7}^{2.3} e^{-W(\delta)/k_BT}\,d\delta$ (cm)	k_{TST}[a] (s^{-1})	$\Delta G^{\ddagger}$[b] (kcal/mol)	$\Delta S^{\ddagger}$[c] (cal/mol·K)
330	2.594×10^4	9.38	3.738×10^{-10}	4.253×10^7	7.23	−27
300	2.473×10^4	8.72	2.382×10^{-10}	4.605×10^7	6.41	−15
270	2.346×10^4	8.35	1.195×10^{-10}	3.430×10^7	5.96	−11
240	2.212×10^4	6.91	2.003×10^{-9}	5.626×10^6	5.63	−8
210	2.069×10^4	6.74	7.590×10^{-10}	2.634×10^6	5.40	−6
180	1.916×10^4	6.14	7.342×10^{-10}	9.142×10^5	5.23	

[a] Calculated using eq 5. [b] Free energy barriers obtained from Figure 7. [c] $\Delta S^{\ddagger} = (\Delta G^{\ddagger}_2 - \Delta G^{\ddagger}_1)/(T_1 - T_2)$. For example, $\Delta S^{\ddagger}$ at 315 K is estimated to be −27 eu.

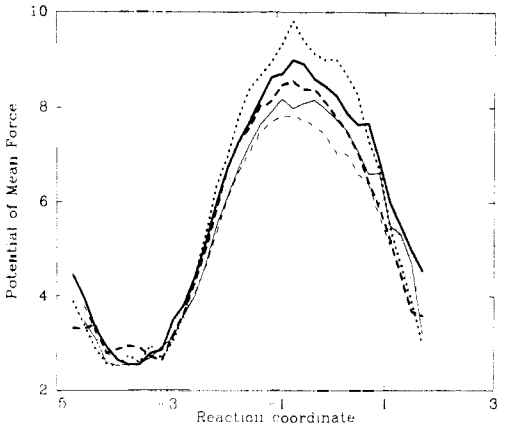

Figure 7. Potentials of mean force at different temperatures. The origin for W is arbitrary and the minima in the heme pocket region have been matched for comparison of barriers: thick dots, 330 K; thick solid, 300 K; thick dash, 270 K; light dots, 240 K; light solid, 210 K; light dash, 180 K.

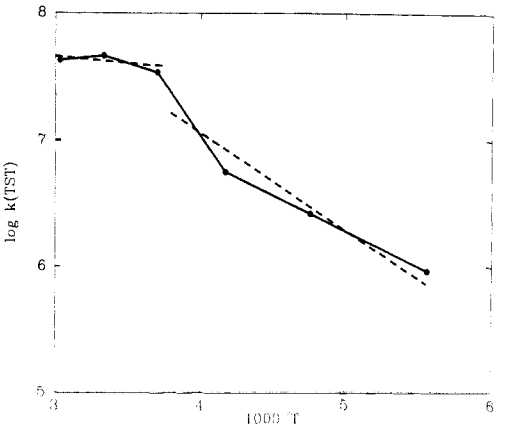

Figure 8. Arrhenius plot for the temperature dependence of k_{TST}.

distribution at the top of the barrier (where $\delta = \delta^+$), and the integral is over the initial state—in this case over the region where the ligand is in the heme pocket. It may be shown that k_{TST} represents a rigorous upper bound to the true (classical mechanical) rate of crossing the barrier.

The average velocity at the top of the barrier was determined by a numerical procedure described earlier,[10] yielding mean absolute velocities of 5.0×10^4 and 3.9×10^4 cm/s at 300 and 180 K, respectively. These are quite close to values predicted for mean thermal crossing velocities for a Maxwell–Boltzmann distribution:[17]

$$\langle\dot{\delta}^2\rangle/(\langle|\dot{\delta}|\rangle = (\pi k_B T/2\mu)^{1/2} \qquad (6)$$

Here μ is the reduced mass along the reaction coordinate. For our definition of δ, this is quite complex to compute algebraically, but is likely to be close to 16 amu, or half the mass of the ligand, since the masses of the ligand and the "gate" atoms are approximately the same. Inserting $\mu = 16$ amu into this equation yields average velocities at 300 and 180 K essentially identical with those determined by the numerical procedure, and the numerically confirmed $T^{1/2}$ temperature dependence can be used to provide estimates for other temperatures. These values, along with those for the remaining parameters in eq 5 and the resulting estimates for k_{TST}, are given in Table III. The numerical values for the terms involving ρ depend upon the chosen zero of energy (which we take to be at the bottom of the heme pocket well), but their ratio is independent of this choice.

The computed temperature dependence of the rate constant is plotted versus $1/T$ in Figure 8. Near 300 K the computed rate is nearly independent of temperature, whereas at lower temperatures a significant slope is observed. The observed slope for the temperature range 180–270 K corresponds to an Arrhenius activation energy E_a of about 5 kcal/mol. The computed rate constant at room temperature (ca. 4×10^7 s^{-1}) is in good agreement with the experimental estimates discussed above. The slowing down of the escape rate at lower temperatures is in qualitative, but not quantitative, agreement with the results of the Illinois group.[1] Potential implications of the unusual temperature dependence will be discussed below.

6. Corrections to Transition-State Theory. Once the potential of mean force has been determined, it is straightforward to compute representative trajectories that start at the bottleneck region and progress forward and backward in time. These allow one to study dynamical features of the reaction that are needed to determine corrections to the transition-state theory rate; these corrections define the transmission coefficient κ.

To carry this out, the system is first constrained to lie near the top of the free energy barrier with a strong umbrella potential having $K = 50$ kcal/mol-A^2 and $\delta_0 = -0.65$. Coordinates and velocities of the system were saved at every tenth time that δ crossed δ_0, and 30 such sets were obtained at 300 and 180 K. These were used as starting conditions for unconstrained trajectories (i.e., with no umbrella potential), which were integrated forward and backward in time for 2 ps in each direction. This creates a small but representative sampling of trajectories that cross the bottleneck region. To the extent that no additional recrossings of the line $\delta = \delta_0$ occur, the transition-state theory rate is accurate.

Corrections to k_{TST} fundamentally arise when trajectories cross the dividing surface more than once, i.e., when the dynamics is not "straight-through" in the transition-state region. For our system, these recrossings invariably occur within 0.2 ps if they are to occur at all within the time scale of our dynamics simulations. (This is equivalent to computing the time-correlation function for the net flux into the final state region,[18] and finding a plateau value after 0.2 ps.) Under these circumstances, the transmission coefficient κ can be determined by weighting each trajectory by its crossing velocity, and counting the number of recrossings:[17]

$$\kappa = \langle|\dot{\delta}|[1 + (-1)^{N+1}]/2N\rangle/(\langle|\dot{\delta}|\rangle \qquad (7)$$

where N is the total number of times each trajectory crosses the dividing surface. Transition-state theory corresponds to $N \equiv 1$.

(17) Bennett, C. H. *Algorithms for Chemical Computation* (ACS Symposium Series); Christofferson, R. E., Ed.; American Chemical Society: Washington, DC, 1977; No. 46. Chapman, S.; Hornstein, S. M.; Miller, W. H. *J. Am. Chem. Soc.* **1975**, *97*, 892.

(18) Chandler, D. *J. Chem. Phys.* **1978**, *68*, 2959.

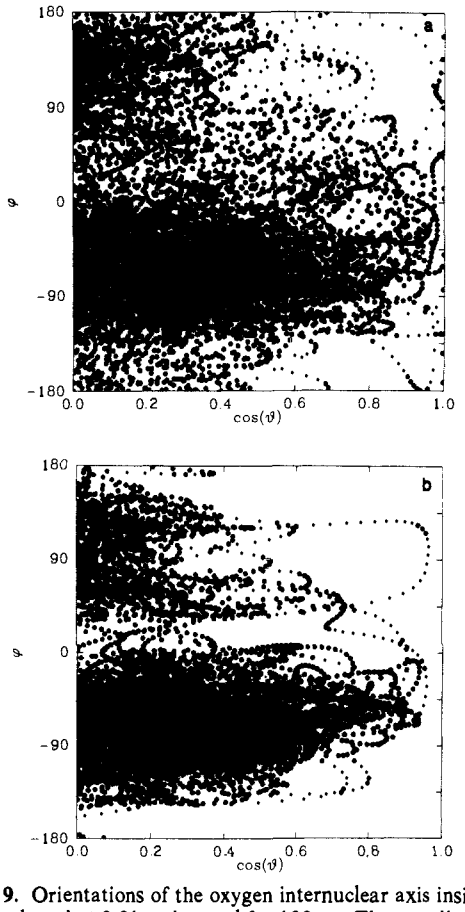

Figure 9. Orientations of the oxygen internuclear axis inside the heme pocket, plotted at 0.01-ps interval for 100 ps. The coordinate system is explained in the text. An isotropic sampling of all orientations would appear uniform in the plot area: (a) 300 K, (b) 180 K.

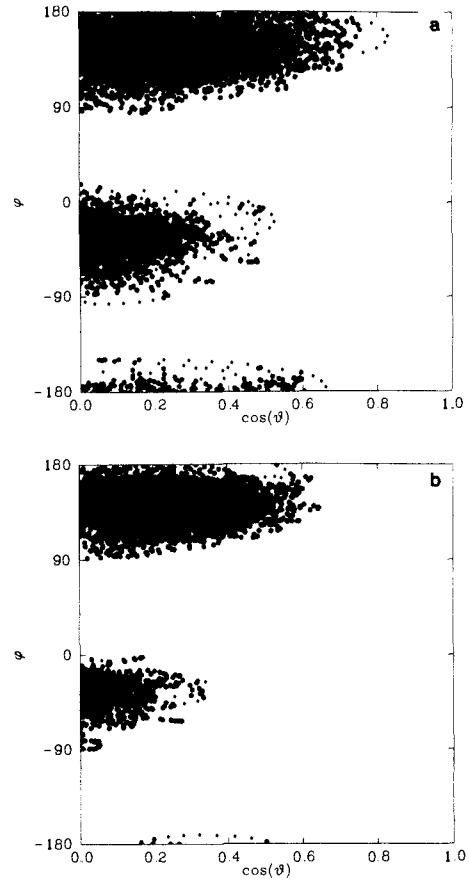

Figure 10. Orientations of the oxygen internuclear axis at the transition state, plotted at 0.01-ps interval for 100 ps: (a) 300 K, (b) 180 K.

Such calculations at 300 K were reported earlier, along with pictures of several of the reactive and nonreactive trajectories.[10] At 300 K, most of the dynamics is indeed "straight-through", and the transmission coefficient is estimated to be 0.91. Things change only a little at 180 K, where we compute $\kappa = 0.81$. Although it is clear that precise estimates of κ require many more than 30 trajectories, our sample of 60 trajectories at two temperatures suggests that, for this particular barrier, corrections to transition-state theory are not large.

Discussion

Although a great deal is known experimentally about the process by which gaseous ligands bind to myoglobin, the task of providing a concrete visualization of the intermediate steps remains formidable. The present calculations provide a detailed model for one of the steps in this process, the escape of the ligand from the heme pocket, and also explore aspects of theory that are applicable to other problems in protein dynamics. The basic computational ideas for obtaining the potentials of mean force have been widely used in earlier condensed matter studies.[19]

Nevertheless, these are still *model* calculations, and it is prudent to begin the discussion by reiterating the limitations of the calculations reported here. First, the escape path we have chosen to study may not correspond in any simple way to phenomenological kinetic events, and may indeed not be the most favorable path out of the heme pocket. Both we[6] and others[20] have identified alternative pathways of ligand escape, and the task of identifying those with the most favorable rate constants remains unsolved. In principle, calculations like those reported here could help to screen potential alternatives. Second, no account of solvation is included in the present results, and the potential consequences of this omission are severe. Solvation effects may change the character and amplitude of the protein fluctuations, especially if ionic interactions are broken in intermediate states, as one recent proposal suggests.[21] In principle, adding explicit solvent to the present simulation is straightforward, although great care will be required to assure that such a description is realistic, especially if salt bridges are to be broken. Such calculations are currently in progress.

In spite of these caveats, the present results offer a significant advance over previous simulations of ligand binding to proteins in obtaining near-statistical convergenge of rate constants for a variety of temperatures. They provide a concrete model in which to explore kinetic aspects of gaseous diffusion in proteins and suggest that temperature extrapolations need to be made with some care. Several interesting points arising from the simulations are discussed in the following paragraphs.

1. Nature of the Geminate Intermediate. Picosecond optical studies of rebinding of dioxygen to myoglobin show significant rebinding on a picosecond time scale from a "geminate" intermediate (state "B" in the kinetic scheme above).[2d,22] This has been termed a "contact pair" state, and may be similar to intermediates seen at low temperatures by EXAFS and infrared spectroscopy.[23] At longer times, an additional intermediate ("C") is observed kinetically, which presumably can explore all of the

(19) Pangali, C.; Rao, M.; Berne, B. *J. Chem. Phys.* **1979**, *71*, 2975. For a review, see: Mezei, M.; Beveridge, D. L. *Ann. N.Y. Acad. Sci.* **1986**, *482*, 1.

(20) Elber, R.; Karplus, M., personal communication.

(21) Westrick, J. A.; Goodman, J. L.; Peters, K. S. *Biochemistry* **1987**, *26*, 8313.

(22) Martin, J. L.; Migus, A.; Poyart, C.; Lecarpentier, Y.; Antonetti, A.; Orszag, A. *Biochem. Biophys. Res. Commun.* **1982**, *107*, 803. Hutchison, J. A.; Noe, L. J. *IEEE J. Quantum Electron.* **1984**, *QE-20*, 1353. Lack of picosecond recombination of dioxygen to Mb was reported by: Cornelius, P. A.; Steele, A. W.; Chernoff, D. A.; Hochstrasser, R. M. *Proc. Natl. Acad. Sci. U.S.A.* **1981**, *78*, 7526.

(23) Chance, B.; Fischetti, R.; Powers, L. *Biochemistry* **1983**, *22*, 3820. Powers, L.; Sessler, J. L.; Woolery, G. L.; Chance, B. *Biochemistry* **1984**, *23*, 5519. Teng, T.-Y.; Huang, H. W.; Olah, G. A. *Biochemistry* **1987**, *26*, 8066. Fiamingo, F. G.; Alben, J. O. *Biochemistry* **1985**, *24*, 7964.

heme pocket region, and perhaps visits other sites inside the protein as well. This intermediate escapes to solvent (where the ligand competes with other ligands to rebind) with a rate of about 10^7 s^{-1}. As illustrated in Figure 3, in our simulation the ligand explores all of what is conventionally called the heme pocket, and escapes on a 10^{-7}-s time scale; this provides a potential model for the nanosecond kinetic intermediate "C".

Figure 9 shows the distribution of the orientations of the dioxygen ligand at 300 and 180 K. Our coordinate system places the z axis perpendicular to the plane of the heme, with the x and y axes along the methine bridge direction. Hence, pyrroles A, B, C, and D are in the first, fourth, third, and second quadrants, respectively. The dioxygen axis generally prefers to be aligned more than 60° away from the heme normal ($\cos\theta < 0.5$), with the oxygen atom further from the heme plane being preferentially pointing toward the direction of pyrrole B ($\phi \approx -60°$). This orientation is rotated relative to that seen in the bound state of MbCO by X-ray crystallography,[9] and the center of mass of the ligand has moved to being (on average) 3.9 Å from the iron atom, compared to 2.4 Å in the bound state. The orientational preference is more pronounced at 180 K than at 300 K; at room temperature, the dioxygen axis adopts a wide range of orientations. The distributions for subsections of the 100-ps trajectory (not shown) are close to those for the full trajectory, and we see no evidence of trapping of orientational intermediates for more than a few picoseconds.

These results correspond closely to those reported earlier by Sassaroli and Rousseau[5] based on energy minimization calculations. The space-filling pictures reported in ref 5 are essentially indistinguishable from those we have made of "snapshots" at various points along our dynamics trajectory.

The volume of the heme pocket accessible to the ligand center of mass is also an interesting parameter in making simple estimates of rate constants for various processes. We can estimate the volume accessible to the center of mass of the ligand from data like that shown in Figure 3. When this trajectory is viewed in three dimensions, it closely approximates a general ellipsoid with principal diameters of 1.4, 1.3, and 1.0 Å, corresponding to a volume of 0.93 $Å^3$. Free (hard-sphere) motion of a particle of mass 32 amu in such a volume yields an estimate of the translational entropy of the ligand inside the pocket: S_{trans} = 15.2 eu, or TS_{trans} = 4.6 kcal/mol at T = 300 K. At 180 K, the effective volume accessible to the center of mass is slightly smaller (0.63 $Å^3$), yielding S_{trans} = 12.9 eu, or TS_{trans} = 2.3 kcal/mol at T = 180 K.

2. Nature of the Barrier to Ligand Escape. All room-temperature studies of rebinding of diatomic ligands to myoglobin show that ligand escape from the nanosecond "geminate" intermediate takes place with a rate constant near 10^7 s^{-1}. This is in good agreement with the value determined here, showing that our model is at least consistent with experimental data. The temperature dependence has been reported only at low temperatures,[1] and as Figure 8 indicates, it is certainly possible that different behavior might be found at higher temperatures. Our preliminary results[10] showed a significant contribution of entropic terms to the barrier at room temperature, and this is borne out by the more extensive calculations reported here.

A fairly simple model can be proposed, which is not unique, but which explains most of what is seen in the calculation. In this model, the ligand must squeeze through a narrow path between two residues which open up (on the average) only enough to just let the ligand escape. Thus, much of the rotational and translation freedom enjoyed by the ligand in the geminate intermediate is lost in ascending the barrier to escape from the protein. We can make only rough estimates of the magnitudes of these effects, but they serve to illustrate what is likely to be involved. The translational entropy in the heme pocket was estimated above to be about 15 eu at room temperature. A freely rotating dioxygen molecule has about 10 eu of rotational entropy at 300 K; Figure 9a suggests that rotational motion in the heme pocket is only partially restricted, so that much of this entropy should be available in the geminate intermediate. Figure 10a shows the orientation distribution at the transition state, where it is clear that very little rotational freedom remains.

Thus it is reasonable to postulate that the dioxygen ligand has 20–25 eu of entropy in the geminate state, and that much of this is lost in the transition state. Rough estimates of the activation entropies, based on the computed temperature dependence of ΔG^+, are given in the final column of Table III. At room temperature, the entropic contribution to ΔG^+ is thus 4–6 kcal/mol, which is a significant fraction of our total barrier of about 7 kcal/mol (see Figure 5). At lower temperatures, these entropic effects become less important as the heme pocket contracts slightly, and the ligand's rotational freedom is also reduced (see Figure 9b). The entropic contribution to ΔG^+ is smaller, and it becomes necessary for the ligand to cross a potential energy barrier of several kcal/mol in order to escape into solution. In a very qualitative chemical language, one might say that the "break" in the Arrhenius plot shown in Figure 8 arises from a change in "mechanism": at low temperatures, the rate is limited by the necessity to cross a potential barrier associated with opening of a gate to the heme pocket. At higher temperatures, the protein becomes more fluid, the barrier to escape is reduced, and the rate of escape becomes limited by the frequency at which the ligand can "find" the proper exit path. If this model is valid, it is likely to be found in many ligand binding events.

Here we have used the temperature dependence of the computed rate constants to estimate the entropy and enthalpy of activation. In principle, it is also possible to estimate the activation energy directly from the ensemble average of the oxygen–globin potential energy distribution along the reaction coordinate. This approach has been successful in earlier studies of tyrosine rotations in the pancreatic trypsin inhibitor,[24] and we reported results of this sort at 300 K in our earlier paper.[10] These results are completely consistent with the conclusion that there is a large entropy contribution to the activation free energy near room temperature. However, in our experience the statistical convergence of properties like $\langle V \rangle$, the mean potential energy, is much worse than for the potential of mean force (cf. Figure 2 of ref 10) so that the method used here seems preferable.

Our model for ligand escape has several features in common with that used by Cotes and Sceats[25] to discuss rebinding of ligands from the geminate pocket. In both models, geometric features of the pocket dominate the reaction dynamics and produce activation barriers strongly influenced by entropic effects. Both models find regimes in which the rate of leaving the geminate pocket (either to rebind to the iron or to escape into solvent) has only a weak temperature dependence, and both models find that motion across the transition state is ballistic, rather than diffusive. Of course, our results on ligand escape say nothing about the correctness of the Cotes and Sceats model for ligand rebinding, and other interpretations of the rebinding kinetics have also been proposed.[1]

Experimental estimates of the enthalpy and entropy of activation near room temperature are not available. If we *assume* a preexponential factor of 6×10^{12} s^{-1}, then an observed rate constant of 10^7 s^{-1} implies an activation free energy of about 8 kcal/mol. Our calculations are in rough agreement with this estimate and suggest that there is no large increase in the protein flexibility on going to the transition state (i.e., we do not see an Arrhenius preexponential factor much larger than 10^{13} s^{-1}). An activation energy of about 12 kcal/mol and a large Arrhenius preexponential factor have been inferred from low-temperature data.[1] Our numbers might be dramatically changed by solvent effects, especially if ionic interactions are formed or disrupted along the escape trajectory. Simulations testing this possibility are currently being planned. Nevertheless, the results presented here support a plausible model for the origin of this escape barrier and demonstrate that (at least under vacuum) rate constant calcula-

(24) Northrup, S. H.; Pear, M. R.; Lee, C.-Y.; McCammon, J. A.; Karplus, M. *Proc. Natl. Acad. Sci. U.S.A.* **1982**, *79*, 4035. McCammon, J. A.; Lee, C.-Y.; Northrup, S. H. *J. Am. Chem. Soc.* **1983**, *105*, 2232.

(25) Cotes, N. J.; Sceats, M. G. *Chem. Phys. Lett.* **1987**, *141*, 405.

tions for ligand binding processes are now feasible. The corresponding ability to study the thermodynamics of these processes through variable-temperature simulations offers new ways to check the validity of dynamical simulations, and to use such simulations to provide a deeper understanding of ligand binding processes.

Acknowledgment. This study was supported by NIH Grant GM39266. We thank John Olson, Teddy Traylor, and Doug Magde for helpful discussions.

Registry No. Dioxygen, 7782-44-7.

Ring Currents in Wholly Inorganic Heteropoly Blue Complexes. Evaluation by a Modification of Evans's Susceptibility Method

Mariusz Kozik,† Nieves Casan-Pastor, Charles F. Hammer, and Louis C. W. Baker*

Contribution from the Department of Chemistry, Georgetown University, Washington, D.C. 20057. *Received February 8, 1988*

Abstract: For seven diamagnetic heteropoly complexes, the difference between the diamagnetic susceptibility of each and that of its 2e heteropoly blue reduction product was measured by the Evans NMR susceptibility method, using a modification that yields very accurate differences. The oxidized forms of the complexes used were α-$[SiW_{12}O_{40}]^{4-}$, α-$[(H_2O)ZnSiW_{11}O_{39}]^{6-}$, α-$[P_2W_{18}O_{62}]^{6-}$, α-$[P_2Mo_3W_{15}O_{62}]^{6-}$, α-$[P_2Mo_6W_{12}O_{62}]^{6-}$, α_1-$[P_2MoW_{17}O_{62}]^{6-}$, and α_2-$[P_2MoW_{17}O_{62}]^{6-}$. In each case the 2e reduction product was *more* diamagnetic than its oxidized parent. The excess diamagnetism is attributable to a ring current of the paired delocalized "blue" electron(s) circulating, under the influence of the imposed magnetic field, in a loop in a plane with a preferred orientation perpendicular to the external field. We are unaware of other ring currents reported for discrete wholly inorganic structures. The magnitude of the additional diamagnetism caused by the ring current depends on the radius of the loop and the number of delocalized electrons circulating. The ring-current diamagnetisms are calculable by Langevin's equation, which yields values that coincide well with the experimental data. Since the delocalization of the added electrons in α-$[SiW_{12}O_{40}]^{6-}$ is almost spherical, its ring current is not dependent on the complex's orientation whereas anisotropy lowers the diamagnetic contribution of the ring current in the Zn complex and in the Wells–Dawson 18-addenda atom derivatives. In isotropic α-$[SiW_{12}O_{40}]^{6-}$ the excess diamagnetism indicates a ring-current radius of 5.4 ± 0.2 Å, which coincides with a delocalization primarily through the outer W–O shell of the complex, in accordance with evolving ^{183}W NMR data. In the Mo derivatives, Mo^{6+} is more easily reduced than W^{6+}. Thus the ring current has a small radius in α-$[P_2Mo_3W_{15}O_{62}]^{8-}$ and a large radius in α-$[P_2Mo_6W_{12}O_{62}]^{8-}$. In each monosubstituted Mo derivative, one added electron is immobilized on Mo^{5+} while the other circulates in the belt(s) of the complex. All of these effects reconcile quantitatively with the observed values, and the results can be applied to the 1e reduction products, yielding corrections to their paramagnetic moments, which make those moments consistent with one another.

Following introduction of ^{183}W NMR for study of heteropolytungstate complexes[1-5] and after important papers from other groups,[6] our laboratory initiated multinuclear NMR investigations of the "heteropoly blue" anions.[7-9] Numerous heteropoly complexes[10-15] can be reduced by addition of various numbers of electrons. The reduction products, which typically retain the general structures of their oxidized parents and are frequently deep blue in color, comprise a potentially important large group of complexes generally known as the heteropoly blues.[15-17] The added ("blue") electrons are "delocalized", according to various time scales, over certain atoms or regions of the structures.[7,18] Heteropoly blues correspond to class II systems in the Robin and Day[15,19] classification of mixed-valence compounds.

The electron delocalization is viewed as operating through two mechanisms: a thermally activated electron hopping process from one addendum (e.g., W or Mo) atom to the next and a ground-state delocalization (gsd),[16,20] presumably involving π-bonding through bridging oxygen atoms from the reduced metal atom to its neighbors. The degree of gsd has been regarded as relatively small, but its existence was required to account for intervalence charge-transfer optical absorption bands.[16] Absence of ESR signals for, and appearance of ^1H NMR signals[15,21] from, a small number of 2e reduction products (plus a semiqualitative evaluation of a magnetic susceptibility[22]) were interpreted as indicating that when there is an even number of blue electrons, their spins are characteristically paired. That postulate is greatly strengthened by a combination of recent NMR investigations[7,9,23] and the present work.

† Current address: Department of Chemistry, Brookhaven National Laboratory, Upton, NY 11973.

(1) Acerete, R. Doctoral Dissertation, Georgetown University, 1981. *Diss. Abstr. Int., B* **1982**, *B42*, 3701.
(2) Acerete, R.; Hammer, C. F.; Baker, L. C. W. *J. Am. Chem. Soc.* **1979**, *101*, 267.
(3) Acerete, R.; Harmalker, S. P.; Hammer, C. F.; Pope, M. T.; Baker, L. C. W. *J. Chem. Soc., Chem. Commun.* **1979**, 777.
(4) Acerete, R.; Hammer, C. F.; Baker, L. C. W. *J. Am. Chem. Soc.* **1982**, *104*, 5384.
(5) Acerete, R.; Hammer, C. F.; Baker, L. C. W. *Inorg. Chem.* **1984**, *23*, 1478.
(6) For example: (a) Minelli, M.; Enemark, J. H.; Brownlee, R. T. C.; O'Connor, M. J.; Wedd, A. G. *Coord. Chem. Rev.* **1985**, *68*, 244. (b) Lefebvre, J.; Chauveau, F.; Doppelt, P.; Brevard, C. *J. Am. Chem. Soc.* **1981**, *103*, 4589. (c) Jeannin, Y.; Martin-Frère, J. J. *J. Am. Chem. Soc.* **1981**, *103*, 1664. (d) Domaille, P. J.; Knoth, W. H. *Inorg. Chem.* **1983**, *22*, 818. (e) Domaille, P. J. *J. Am. Chem. Soc.* **1984**, *106*, 7677. (f) Brevard, C.; Schimpf, R.; Tourné, G.; Tourné, C. M. *J. Am. Chem. Soc.* **1983**, *105*, 7059. (g) Finke, R. G.; Droege, M. W. *Inorg. Chem.* **1983**, *22*, 1006. (h) Finke, R. G.; Rapko, B.; Saxton, R. J.; Domaille, P. J. *J. Am. Chem. Soc.* **1986**, *108*, 2947.
(7) Kozik, M.; Hammer, C. F.; Baker, L. C. W. *J. Am. Chem. Soc.* **1986**, *108*, 2748.
(8) Kozik, M.; Hammer, C. F.; Baker, L. C. W. *J. Am. Chem. Soc.* **1986**, *108*, 7627.
(9) Kozik, M.; Baker, L. C. W. *J. Am. Chem. Soc.* **1987**, *109*, 3159.
(10) Baker, L. C. W. In *Advances in the Chemistry of Coordination Compounds*; Kirschner, S., Ed.; Macmillan: New York, 1961; p 608ff.
(11) Weakley, T. J. R. *Struct. Bonding (Berlin)* **1974**, *18*, 131.
(12) Evans, H. T., Jr. *Perspect. Struct. Chem.* **1971**, *4*, 1.
(13) Souchay, P. *Ions Minéraux Condensés*; Masson et Cie: Paris, 1969.
(14) Tytko, K. H.; Glemser, O. *Adv. Inorg. Chem. Radiochem.* **1976**, *19*, 239.

0002-7863/88/1510-7697$01.50/0